TAL TECH
SCHOOL OF SCIENCE

Visualising the Milky Way response to the infall of the Large Magellanic Cloud

Bachelor's Thesis

Student: Daniel Nurme
Student code: 213487YAFB
Supervisor: Sven Põder, PhD, Researcher, NICPB
Co-Supervisor: María José Benito Castaño,
PhD, Visiting Research Fellow, Tartu Observatory,
ERA fellow, Instituto de Astrofísica de Canarias
Curriculum: Applied Physics

Tallinn 2026

TAL TECH
LOODUSTEADUSKOND

Visualisatsioonid Linnutee galaktika vastutoimest Suure Magalhãesi Pilve lähenemisele

Bakalaureusetöö

Üliõpilane: Daniel Nurme
Üliõpilaskood: 213487YAFB
Juhendaja: Sven Põder, PhD, Teadur, KBFI
Kaasjuhendaja: María José Benito Castaño,
PhD, Külalisteadur, Tartu Observatoorium,
ERA stipendaat, Instituto de Astrofísica de Canarias
Õppekava: Rakendusfüüsika

Tallinn 2026

Author's declaration of originality

I hereby declare that I have written this thesis independently and the thesis has not previously been submitted for defence. All works and major viewpoints of the other authors, data from sources of literature and elsewhere used for writing this paper have been properly cited.

Author: Daniel Nurme
[Signature, date]

The thesis complies with the requirements for bachelor's theses.

Supervisor: Sven Põder
[Signature, date]

Permitted to the defence.
Chairman of the defence committee:
[Signature, date]

Table of contents

List of abbreviations and terms

DM	Dark matter
CDM	Cold Dark Matter
FDM	Fuzzy Dark Matter
HDM	Hot Dark Matter
MW	Milky Way
LMC	Large Magellanic Cloud
Gyr	Gigayear (10^9 years)
DF	Dynamical friction
Galactic coordinate system	A coordinate system where the origin of the coordinates is centered on the Sun
Galactocentric coordinate system	A coordinate system where the origin of the coordinates is centered on the center of the Milky Way galaxy
Galactic plane	A 2 dimensional plane which slices the Galactic disc into two halves (top and bottom). Denotes where most of the Galaxy's mass lies. Perpendicular to the Galactic poles

1 Introduction

Understanding the true nature of dark matter plays a critical role in developing an accurate model to describe how the Universe evolved into the state observed today. Despite extensive experimental searches, the dark matter particle remains elusive. Due to the difficulties in detecting dark matter directly, astrophysical and cosmological probes have been implemented in the search for this particle. The constraints on dark matter are inferred through its gravitational interactions with surrounding matter, making the probes reliant on looking for gravitational interactions between massive objects.

To describe this behaviour, observations from cosmological scales have resulted in the ΛCDM model, which is currently the standard cosmological model, being able to predict, with reasonable accuracy, how the Universe evolved into its observed state [1]. While the model successfully explains how the large-scale structure of the Universe came to be, it is less constrained on Galactic and subgalactic scales [2]. In particular, the ΛCDM model predicts that galaxies reside in dark matter halos, which are thought to contain substructure in the form of subhalos. As the abundance of subhalos depends on the particle properties of dark matter, efforts are being made to detect them.

In recent literature, the most popular methods for dark matter halo detections include detections of stellar streams and gravitational lensing [3, 1]. Additionally to the previously mentioned, recent studies have demonstrated that, while detection of stellar wakes are still in its early days, it proves as a promising addition to the already existing methods [4].

This thesis aims to create a transformation tool which is able to visualise windtunnel-style simulation data and present it as it would appear when viewed from Earth. Additionally, using the results produced by the tool can help assess the possibility of using this tool to discriminate between cored and cuspy dark matter halo profiles.

To address these aims, the following sections give an overview of the theoretical background of the dark matter problem, outline the aims, expand on the simulation setup used in this thesis as well as explain the transformation pipeline and Mollweide projection for the visualisation tool. Finally, the results of the tool are shown and the implications for dark matter research are discussed. The work is concluded with a summary of the findings.

2 Theoretical background

Cosmology is a branch of physics which aims to study the Universe as a whole. Observations from the past century have significantly altered our understanding of the Universe and how it came to be. As the observational evidence points towards an evolving Universe, several mysteries still remain about how exactly the Universe evolved into the current state. Among the myriad of cosmological puzzles, dark matter (DM) remains one of the most enduring problems today. Due to the nature of dark matter, searching for the particle has proved to be a challenge, as any form of interaction with the electromagnetic (EM) spectrum is yet to be detected. Studies on direct DM interaction with baryonic matter have been conducted, though this avenue of research has yet to give results. The only observationally confirmed interaction comes from surveying the large scale structure of the Universe, which suggests that DM interacts gravitationally. This has garnered significant attention from the scientific community in the form of research into indirect DM observations through gravitational interactions.

2.1 A brief history

In the 1930s, Fritz Zwicky, a Swiss-American physicist was examining the redshifts of galaxies in the Coma cluster [5], a cluster of galaxies within the Coma Berenices constellation. Zwicky noticed a discrepancy within the dispersion of radial velocities in the cluster's galaxies. He noted that the visible matter within the cluster did not provide a large enough gravitational pull to keep the cluster together at such speeds [6]. Earlier, in 1931, Edwin Hubble and Milton Humason [7], who had published the data Zwicky was now working on, had also noticed the discrepancy. It was Zwicky who had applied the virial theorem[1] to estimate the mass of the cluster based on these new results [9]. Zwicky reached a result which suggested that the mass of the Coma cluster is 400 times larger than what calculations from visual observations would give [5, 9]. Though later research would put the number much lower, Zwicky had made an important discovery which helped shape our understanding of the Universe.

In 1970, a second discovery was made by Vera Rubin and Kent Ford, which prompted the scientific community to look back on the work of Zwicky. Along with the $21\ \mathrm{cm}$ hydrogen emission data from radio astronomers, Rubin and Ford managed to map the dynamics of M31 with higher accuracy than had been achieved before [9]. It was within those measurements that Rubin noticed that the rotation curve for M31 remained flat at a large distance from the nucleus (see Figure 1) [10].

[1] The virial theorem, first derived in 1870 by Rudolf Clausius, in the context of the kinetic theory of gases, relates the total kinetic energy of a steady system to the potential energy and makes it possible to find the mass of a kinematic system [8]. However, this is not a very accurate method, when only partial information is known about a system [6].

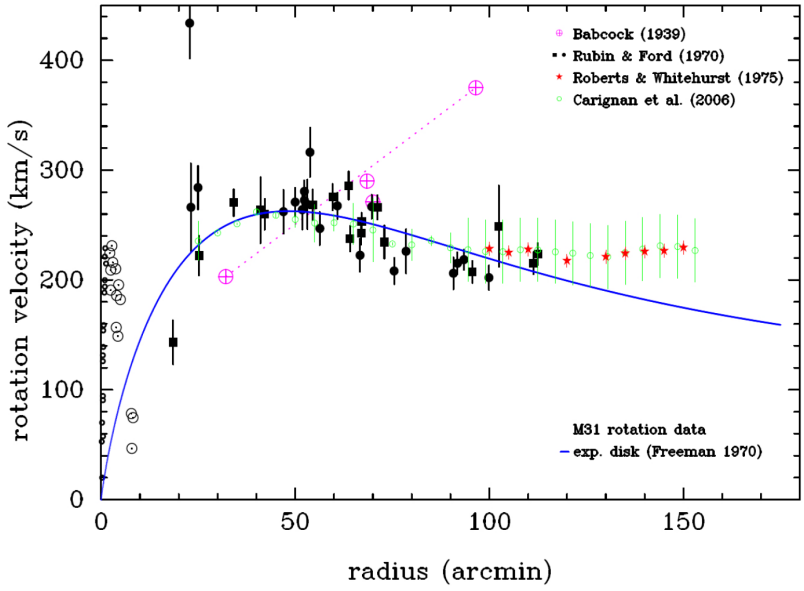

Figure 1. Rotation curve data for M31 (Andromeda galaxy) over the years. Purple - Babcock (1939), Orange - van de Hulst et al. (1958), Black - Rubin and Ford (1970), Red - Roberts and Whitehurst (1975), Green - Carignan et al. (2006). Blue line, given by Freeman (1970) represents the maximum disk rotation curve of an exponential disk. [11].

These discoveries led the scientific community to come up with an explanation for the observed data. The problem became known as the dark matter problem, due to the observations suggesting that the discrepancy was caused by additional invisible mass within the systems [12, 13].

2.2 Dark matter

The DM problem can be summarised as a problem of the missing mass in the Universe. "Dark matter" serves as a provisional name for the problem and describes only the property of the missing mass being invisible to us. Today the existence of DM is well-established in modern physics. It is supported by a wide range of observational probes across diverse cosmological and astrophysical scales, a few of which were mentioned in Section 2.1. From being a curious byproduct in cosmological studies in the 20th century, DM has grown into a multidisciplinary subject spanning cosmology, astrophysics, and particle physics. Despite extensive experimental efforts, particle searches for DM have so far failed to detect a DM particle, and therefore its microphysical properties remain poorly constrained [14]. Thus, astrophysical and cosmological observations are currently the only effective methods to probe the nature of DM.

While it is unknown what DM consists of, its behaviour on very large scales has been well constrained. Observations of the large-scale structure in the past 30 years indicate that DM behaves effectively as a collisionless component that is consistent with the Cold Dark Matter (CDM) paradigm. A "cold" particle is described as a particle which has a non-relativistic thermal velocity and would not suppress structure formation on any scale relevant for galaxy formation [15,

2]. From the visible structure it is inferred that a thermally cold DM particle would have had the time to organise into the structure observed today in the Universe.

Discovery of the Cosmic Microwave Background (CMB) radiation, coupled with the emergence of CDM and dark energy[2], has led to the establishment of the ΛCDM model. The ΛCDM is currently our standard cosmological model, being able to account for numerous cosmological and astrophysical observations. The model predicts how DM acts on large-scale structures, amassing into filament-like shapes, generating a web-like structure and leaving voids in between, also known as the cosmic web [16]. Despite its successes on large scales, the ΛCDM model still faces many open questions at Galactic and subgalactic scales, where it is currently poorly constrained by observations. Many DM candidates have been proposed (such as warm dark matter (WDM), self-interacting dark matter (SIDM), and fuzzy dark matter (FDM))[3] which all act like CDM on large scales, but behave differently at smaller scales. Specifically, different DM models proposed in the literature (CDM and its extensions) are expected to leave characteristic effects on the shapes and substructure of DM halos (see Section 2.3). Consequently, the characterisation of these halos is a powerful indirect probe to study the fundamental nature of DM.

2.3 Dark matter halos

DM halos are concentrated, gravitationally bound "clumps" of DM. Galaxies are thought to reside in massive DM halos [12, 13], where the host halo of a galaxy contributes most of the mass inside the system and therefore dominates its gravitational potential (Figure 2). The dynamics of the galaxy are therefore largely governed by the halo except in the inner regions, where baryonic matter starts to dominate [4]. The DM halos are thought to reach out much further than the luminous material within the galaxy, connecting with the halos of nearby galaxies, and forming a cosmic web of matter [1].

The distribution of dark matter within these halos is described by a density profile, which is a function that describes how mass density is distributed in space [20]. As DM halos are highly non-linear structures, the distribution of DM within the halos is studied using N-body and hydrodynamical simulations. These simulations are able to reproduce the large-scale structure of the Universe, but the results at scales smaller than $\sim 0.1\ \mathrm{Mpc}$ and masses smaller than $\sim 10^{11}\ \mathrm{M}_{\odot}$ differ from observations. This discrepancy is called the core-cusp problem, where simulations predict a cuspy central density profile while observations suggest a shallower core profile. This problem is further exacerbated by an uncertainty over whether baryonic matter plays a role in shaping the halo profile, as this could possibly help explain the discrepancy [2]. While many different profiles have been adopted in the literature, this work focuses only on the Hernquist

[2]While dark energy is not within the scope of this work, it is understood as the force driving the accelerated expansion of the Universe [1]

[3]This thesis will only focus on CDM.

[4]This holds true for galaxies such as the MW. Dwarf galaxies below a certain mass threshold have been observed to have negligible stellar masses in the inner regions compared to the mass of the DM halo [17, 18].

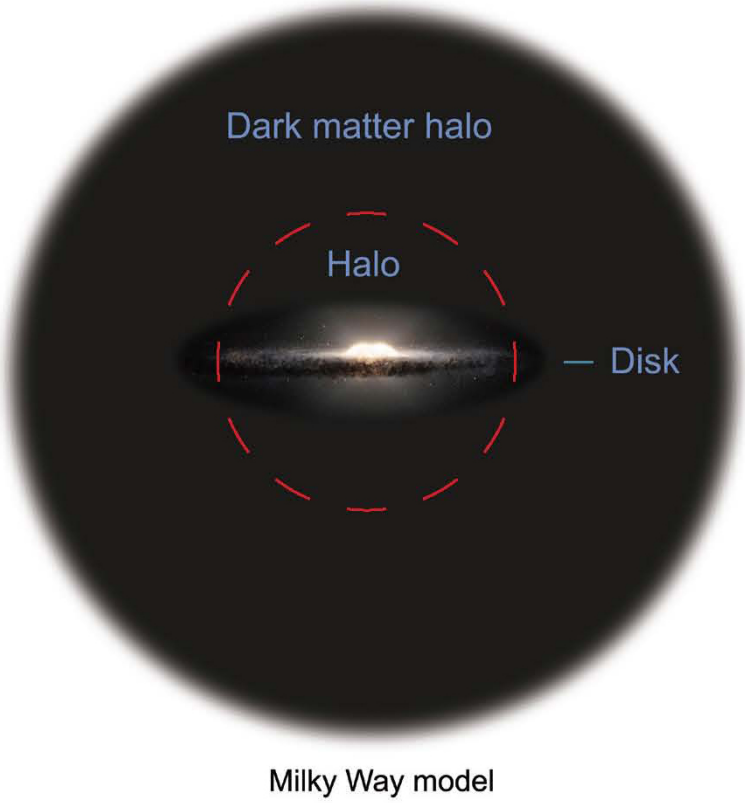

Figure 2. Illustration of a DM halo surrounding a Galactic disk [19].

(cuspy) and Plummer (core) profiles (Figure 3). The Hernquist density profile can be written as

$$\rho(r)_H = \frac{M}{2\pi}\frac{r_s}{r}\frac{1}{(r+r_s)^3} \tag{2.1}$$

where M is the mass of the galaxy and r_s is the scale length [21]. The values for M and r_s for the purpose of this thesis were taken from Foote et al. [22] to be $M_{lmc} = 1.8 \cdot 10^{11} M_\odot$ and $r_s = 20\ \mathrm{kpc}$ (mass and scale length of the LMC, respectively). Additionally, the Plummer density profile can be written as

$$\rho(r)_P = \frac{3M}{4\pi r_s^3}\left(1+\frac{r^2}{r_s^2}\right)^{-\frac{5}{2}} \tag{2.2}$$

where the value of M remains unchanged, but r_s needs to be calculated [23]. The scale length is calculated as

$$r_s = 1.62\ \mathrm{kpc} \times \left(\frac{\mathrm{M}}{10^8 \mathrm{M}_\odot}\right)^{\frac{1}{2}} \tag{2.3}$$

as was done in Põder et al. [24]. When calculated with the mass of the LMC, the scale length becomes $r_s \approx 68.7\ \mathrm{kpc}$.

Based on the ΛCDM model, DM halos grow through a process called hierarchical clustering where small halos merge into bigger ones and continue to merge with smaller halos [14]. An additional mechanism of halo growth is when matter and DM are accreted along the filaments of the cosmic web into the DM halos. Though it is expected that DM halos are disrupted and absorbed into the host galaxy's halo during infall, several such satellite halos survive and form

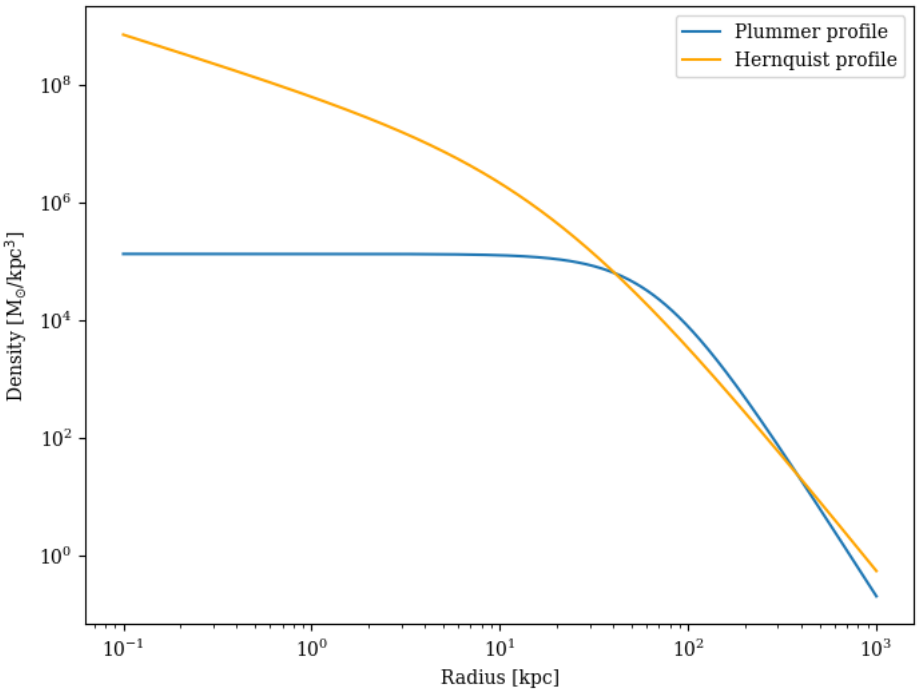

Figure 3. Plummer (core) and Hernquist (cuspy) density profiles for the LMC.

gravitationally bound subhalos within the host halo. The population size of these subhalos is a direct consequence of the particle properties of DM. Characterising the abundance of subhalos on subgalactic scales is one of the most important challenges of the ΛCDM paradigm [1].

Addressing this challenge is complicated by the non-interacting properties of DM, which make direct observations of DM halos essentially impossible. Instead, various indirect observational probes have been used, relying on the detection of visible matter which responds to the gravitational influence of DM. One example is the detection of stellar streams. These are structures formed when small galaxies or globular clusters get tidally destroyed by the gravitational field of the host galaxy and trace thin stellar filaments around the Galactic disc. These streams can be detected via photometric data and used to detect various phenomena within a galaxy, such as dark matter detection, accretion history and Galactic substructure [3]. Other studies have focused on using gravitational lensing. It is a method which relies on a background light source, such as a distant galaxy, to line up with a DM halo source. The lensing effect produced by the distortion of spacetime due to the gravitational mass of the object in the foreground allows us to calculate the lensing mass. Simulating various lensing scenarios, it is possible to infer the nature of the DM halo structure of the lensing mass by comparing the simulation results to observations [1].

2.4 Stellar wakes

The detection of stellar wakes is a new and promising method for inferring the presence of DM subhalos orbiting the Milky Way and characterising the properties of known luminous satellites (e.g., dynamical mass). Stellar wakes are structures induced by massive perturbers as they move

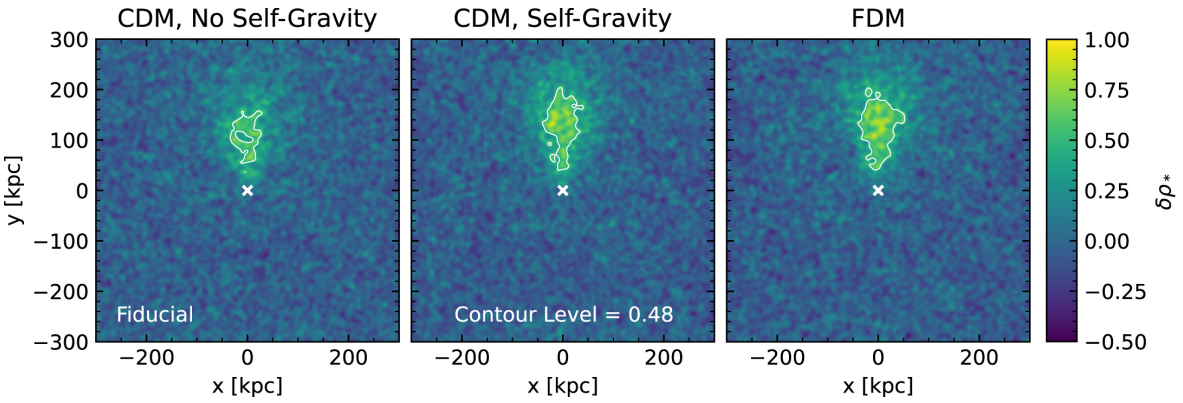

Figure 4. Stellar wake simulations from the paper of Foote et al. [22] Overdense regions of stars created by the perturbations from the LMC in the windtunnel simulation after $0.7\ \mathrm{Gyr}$ of integration. In each scenario, areas with an overdensity greater than the half-max of the CDM with self-gravity are marked by a white contour [22].

through a stellar medium, pulling stars into an overdensity trailing behind the perturber during this process. These structures are expected to have many observable components. The most obvious is an overdensity of stars trailing behind the perturber (Figure 4), although perturbations in the stellar velocity field are also expected. The overdense region following the perturber starts pulling back on it, making the perturber lose angular momentum and energy - an effect called dynamical friction (DF) [25]. This is why, in literature, stellar wakes have also been called dynamical friction wakes (e.g., Foote et al. [22]).[5]

As mentioned in Sections 2.2 and 2.3, the ΛCDM model predicts the existence of DM subhalos within subgalactic scales. Though incredibly difficult to detect, stellar wakes can be used to discover dark subhalos (subhalos without a stellar counterpart) and identifying such wakes would provide important constraints to DM microphysics.

A popular testbed for the detection of stellar wakes has been the LMC. Work has already begun to detect and analyse the wakes behind luminous MW satellites, such as the LMC studies carried out by Gavarito-Camargo et al. [26] and Foote et al. [22]. A wake has tentatively already been detected trailing the LMC as seen in the work of Conroy et al. [27]. As the largest of the MW's satellites undertakes its first infall [28], the resulting response from the MW provides a unique opportunity to detect the DM halo of the LMC and infer its properties.

[5]Dynamical friction falls outside the scope of this work and will not be discussed.

3 Aims of the thesis

Two goals were set for this thesis:

- Create a visualisation tool to transform wakes simulated in a windtunnel box into a Galactic reference frame,
- Assess whether the stellar wake of the LMC can be used to discriminate between cored and cuspy DM halo profiles.

The main goal of the thesis is to create a Python visualisation tool, which is developed according to the Foote et al. [22] procedure. The simulation results as well as the validity of the transformation tool are compared against the results of Foote. Finally, the visualisation results of the Hernquist and Plummer density profiles are compared in the context of the core-cusp problem. This allows us to investigate whether stellar wakes can be used to differentiate between different density profiles (Plummer vs Hernquist). In doing so, this thesis extends the work in Põder et al. [24] and contributes to wake studies more broadly. The work of Põder et al. [24] did not describe the effect of different density profiles on their simulated wakes; the present work addresses this by showing the differences in an observational frame of reference.

4 Methodology

One of the goals of this thesis was to create a tool to efficiently visualise the structure of the stellar wakes in DM simulations using Python. The key step in this visualisation process is transforming the wake into Galactic coordinates, so that the morphology of the wake can be compared with observational data, which is where the value of this tool lies. The code was built from the ground up and simulated datasets were used to verify the results against the work of Foote et al. [22]. The simulations replicate the MW's stellar halo response to the LMC's gravitational potential as the satellite galaxy passes through the MW's stellar halo during its first infall event [28]. Simulated data used in this work are not generated by the author, but are used for the purpose of the creation of the transformation tool. Section 4.1 explains the sources, processes, and parameters used to acquire the data. Section 4.2 describes the coordinate transformation pipeline and the steps required to present the data in a Galactocentric frame of reference. Section 4.3 describes the steps needed to project the data onto a Mollweide projection.

4.1 Simulated datasets

Stellar wakes obtained in windtunnel simulations are not merely idealised constructs, but have been shown to reproduce main features of wakes found in more realistic galaxy simulations [22]. Therefore, the windtunnel setup provides a controlled and physically meaningful framework to study these perturbations.

The wake simulations used in this work are made using PKDGRAV3 [29], which is a versatile cosmological N-body code. The simulation is a windtunnel-style N-body simulation which simulates a massive perturber moving through a homogeneous medium, in this case, the LMC moving through the Milky Way's outer boundary. The setup is similar to the one in Põder et al. [24], though on a larger scale. The simulation contains 512^3 stellar particles and 512^3 DM particles and the simulated medium is a box with equal side lengths of $L = 600\ \mathrm{kpc}$ and periodic boundary conditions on all sides. The coordinates are defined in a range $x, y, z \in [-300, 300]$ and the simulation takes place in the rest frame of the perturber. Any particle moving further than $x < -300\ \mathrm{kpc}$ in the x-direction will reappear at the boundary at $x = 300$. The x-axis of the simulation box acts as the primary direction of the LMC's resultant velocity vector, which will be a useful reference point in the upcoming transformation process. To simulate the motion of the LMC, a wind of stellar and DM particles is introduced, where the particles are moving at a velocity of $-v_x$. The stellar wind particle velocity is approximated to $313.6\ [\mathrm{km/s}]$ as was done in Foote et al. [22]. Similarly to Foote, the gravitational potential in the simulation is described by an external stationary Hernquist potential at the center of the simulation volume. For the purpose of comparison, an

	$r[\,\mathrm{kpc}]$	$v[\,\mathrm{km/s}]$	$\rho_{star}[\,\mathrm{M_\odot/kpc^3}]$	$\sigma_{star}[\,\mathrm{km/s}]$	$N_\star$
Simulation parameters	70	313.6	5.818×10^{-3}	90	512^3

Table 1. Simulation parameters for the stellar wind. With the exception of $N_\star$, most of the parameters have been adopted from Foote et al. [22], while $N_\star$ is adopted from Põder et al. [24]

additional Plummer profile simulation is made with the same simulation parameters (discussed in Section 5.2). The data is simulated with $0.7\ \mathrm{Gyr}$ of integration time, ensuring that the wake has time to form, but also ensuring wake particles which have already interacted with the potential do not circle back to interact with the potential again. While Foote et al. [22] compared three different types of CDM particles (CDM with no self-gravity, CDM with self-gravity, and FDM), this thesis focuses purely on reproducing the results with the CDM with self-gravity model.

Table 1 describes the simulation parameters for the stellar wind. It's important to note that the stellar count for this work's simulation is ~ 4 orders of magnitude higher than in the Foote simulation (1.342×10^8 vs $\sim 1.2 \times 10^4$ respectively). This means that this work's simulations acquire a higher resolution than those of Foote.

The LMC trajectory data is taken from Vasiliev et al. [30], which studied the kinematics of objects and globular clusters in and around the Milky Way using the Gaia Early Data Release 3 (EDR3). The trajectory data is simulated between $t_{start} = -5$ Gyrs and $t_{end} = +0.25$ Gyrs. This dataset gives the assumed location of the LMC in a Galactocentric frame in XYZ coordinates.

The overdensity of the stellar wake trailing behind the gravity potential is calculated as

$$\delta\rho = \frac{\rho}{\bar{\rho}} - 1 = \frac{\Delta\rho}{\bar{\rho}} \tag{4.1}$$

which measures the relative change of density compared to the input stellar wind density. If the density is higher than the background density, then the area is considered overdense, otherwise it is considered underdense [22]. The results of the simulations can be seen in Figures 11a and 11b.

4.2 Reference frame transformations

Since the simulations are run in a frame of reference centered on the LMC, a set of rotations and translations are needed to transform the simulation box into a Galactocentric reference frame. This significantly simplifies the final reference frame transformation into a Mollweide projection. As such, the next steps describe how the simulation coordinates are transformed to match the LMC's real position in orbit around the MW.

4.2.1 Rotation

A key component in the reference frame transformation pipeline is the derivation of rotation matrices. A rotation matrix is a transformation matrix that rotates a set of vectors around one of its axes by a given angle. This process preserves the lines, angles and lengths of the elements

within the matrix [31].

Before setting up the actual rotation pipeline, a visual test was constructed to get a simplified view of the rotation process and check the validity of the procedure. This entailed plotting the orbit of the LMC in a Galactocentric frame of reference and projecting it onto the xy, xz, and yz planes as seen in Figure 5. Then a 3D vector ($v\,\vec{}_{\rm lmc}$), originating from the LMC's current day position, which was tangential to the orbit trajectory, was added. The direction of motion of the LMC in the simulation box was depicted as a dashed line ($v\,\vec{}_{\rm sim}$) along the x-axis. In all figures, the dashed line represents the direction of motion of the LMC.

In order to rotate the test set, the angles between the simulation's velocity vector $v\,\vec{}_{\rm sim}$ and LMC's real velocity vector $v\,\vec{}_{\rm lmc}$ need to be identified.

A total of 2 rotations (yaw and pitch) and therefore 2 angles are needed to rotate the set of data to any desired orientation. For this, the rotations around the z and y-axis were chosen. The first angle α around the z-axis is found by calculating the dot product between the x and y components of $v\,\vec{}_{\rm sim}$ and $v\,\vec{}_{\rm lmc}$.

$$v\,\vec{}_{\rm sim} \cdot v\,\vec{}_{\rm lmc} = |v\,\vec{}_{\rm sim}||v\,\vec{}_{\rm lmc}| \cos\alpha \ , \tag{4.2}$$

$$\alpha = \arccos\left(\frac{v\,\vec{}_{\rm sim} \cdot v\,\vec{}_{\rm lmc}}{|v\,\vec{}_{\rm sim}||v\,\vec{}_{\rm lmc}|}\right) \tag{4.3}$$

Performing the rotation $R_z(\alpha)$ outputs a new rotated vector $v'\vec{}_{\rm sim}$.

$$\begin{bmatrix} \cos\alpha & -\sin\alpha \\ \sin\alpha & \cos\alpha \end{bmatrix} \times \begin{bmatrix} v_{x,\rm sim} \\ v_{y,\rm sim} \end{bmatrix} = v'\vec{}_{\rm sim} \tag{4.4}$$

Now the angle β around the y-axis can be found, now using all 3 components (v_x, v_y, v_z) of vectors $v\,\vec{}_{\rm lmc}$ and $v'\vec{}_{\rm sim}$.

Now that the angles α and β have been found, it is possible to construct the rotation matrix R which will rotate the data to its desired orientation.

$$R = R_z(\alpha) \times R_y(\beta) \tag{4.5}$$

$$R = \begin{bmatrix} \cos\alpha & -\sin\alpha & 0 \\ \sin\alpha & \cos\alpha & 0 \\ 0 & 0 & 1 \end{bmatrix} \times \begin{bmatrix} \cos\beta & 0 & \sin\beta \\ 0 & 1 & 0 \\ -\sin\beta & 0 & \cos\beta \end{bmatrix} \tag{4.6}$$

Performing a matrix multiplication with R and $v\,\vec{}_{\rm sim}$ results in a rotated reference frame with a resultant velocity vector $v''\vec{}_{\rm sim}$ which has now become collinear with $v\,\vec{}_{\rm lmc}$, as seen in Figure 5.

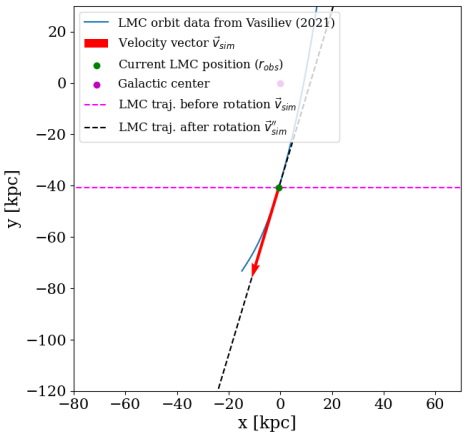

(a) Rotation before and after as seen in the xy plane.

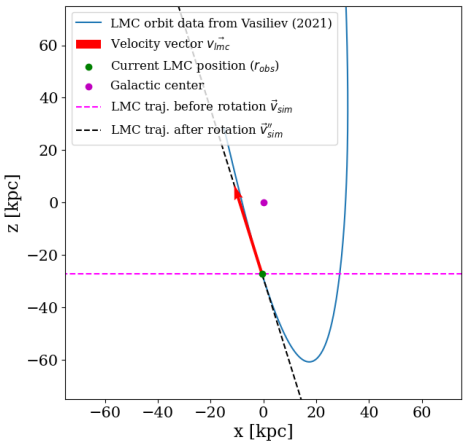

(b) Rotation before and after as seen in the xz plane.

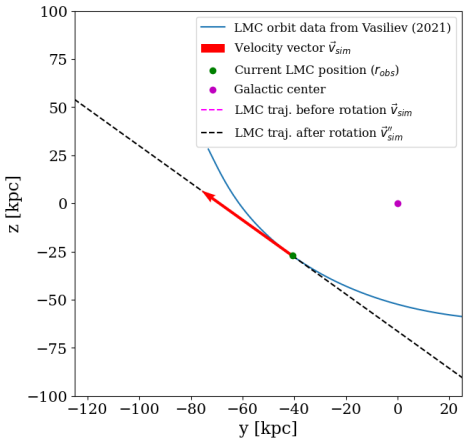

(c) Rotation before and after as seen in the yz plane. The yz plane lacks a *before* dashed line, as the line would be orthogonal to the viewer.

Figure 5. Visualising the transformation of the simulation box (dashed line) before and after rotation.

Once the initial rotation tests were carried out and verified, the procedure described above was generalised and implemented as a Python code routine. This routine takes an arbitrary velocity vector as input and constructs a rotation matrix that aligns the 3D Cartesian positions with that vector. An additional condition was added to the angle finding procedure which checks whether the required rotations are positive or negative in order to take into account that the rotation matrices used in this work are all defined as counterclockwise rotations.

With the rotation procedure validated and generalised, the stellar wake in the box simulation was rotated. Following the procedure of Foote et al. [22], it was rotated using the LMC's velocity vector $v\,\vec{}_{\rm lmc}$ when it was at a Galactocentric distance of $r_{70} = 70\ \mathrm{kpc}$. In the article of Garavito-Camargo et al. [26], it is reasoned that this value was chosen due to the stellar response of the stellar wake being most easily observed at that distance, giving maximum stellar density data without

being obscured by interstellar clouds or the Sagittarius stream. The trajectory data contained two instances where the LMC was simulated to have been at a radial distance of r_{70}, however, only one of those points is usable in this context, as the second point can be eliminated on account of it being a future orbit prediction.

4.2.2 Translation

After the simulation box has been rotated, the center point of the gravitational potential in the box is still situated at the origin of the coordinates (as seen in Figure 6). In order to finalise the transformation, a set of translations needs to be applied to the LMC box simulation [22].

The translation process serves two purposes. The first one is to match the simulated LMC potential with its current day position in the Galactocentric frame. The second one is to match the position of the simulated stellar wake with the observed stellar wake within the LMC orbit at a Galactocentric distance of r_{70}. This ensures realism as the simulation background parameters were chosen to mimic the ambient conditions of the MW at this distance. Thus, the goal was to translate the simulation box to r_{obs}, and from there, project it onto an extension of the vector originating from r_{70} so that the stellar wake would match up with the orbit of the LMC as closely and accurately as possible (see Figure 6).

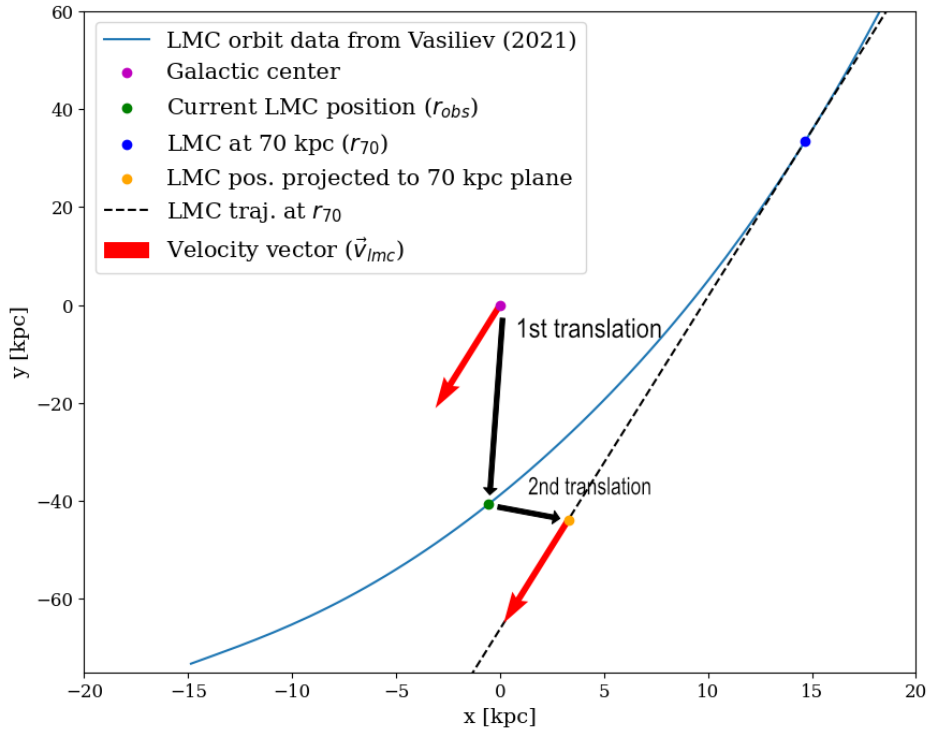

Figure 6. Translation procedure of the simulation box.

The translation pipeline was then carried out as follows: the simulation box was translated to the LMC's current-day position. From there, an orthogonal vector was needed for the final translation from the current-day's position to the destination position. This was found using orthogonal

decomposition, which can be written as

$$(\vec{a} \cdot \hat{v_N}) \times \hat{v_N} = \left(\vec{a} \cdot \frac{\vec{v}}{|\vec{v}|} \right) \times \frac{\vec{v}}{|\vec{v}|} = \vec{d_{\parallel}} \tag{4.7}$$

where $\vec{a}$ is the vector connecting r_{70} and r_{obs}, $\hat{v_N}$ is the unit vector in the direction of $\vec{v_{70}}$, and $\vec{v} = \vec{v_{70}}$ [32]. The result of equation 4.7 is $\vec{d_{\parallel}}$, which is the parallel component to $\vec{a}$. Now, $\vec{a}$ is decomposed as $\vec{a} = \vec{d_{\perp}} + \vec{d_{\parallel}}$, which can now be written as

$$\vec{d_{\perp}} = \vec{a} - \vec{d_{\parallel}}. \tag{4.8}$$

Thus, $\vec{d_{\perp}}$ contains the necessary information to perform the final translation to the destination point. As seen in Figure 6, the simulation box has now undergone a series of transformations and can now be projected into a Mollweide projection.

4.3 Mollweide projection

The final part of visualising the stellar wake is transforming the reference frame into a Mollweide projection. An additional change to the data is needed before plotting it. As explained in Foote et al. [22], the influence of the DM self-gravity on the wake is best observed at a distance of $70 - 100\,\text{kpc}$. If this argument is to be extended to the stellar wake, the best observational signatures should be seen at that distance. As such, a cut of the data was made at a radial distance from the MW's center, between $70 - 100\,\text{kpc}$ and the resulting dataset was used to plot the wake. Finally, using Astropy's `Skycoord` class, the Galactocentric coordinates are transformed into Galactic coordinates. The results are then projected in an all-sky Mollweide projection, which gives a 2D approximation of how an Earth-based observer might see the forming structures in the sky. The Mollweide projection is a pseudocylindrical equal-area projection type which maps the celestial sphere from the inside onto a 2D plane. While this projection fails in accurately portraying angles and shapes, it succeeds in portraying proportions in area, making it a preferred projection for cosmologists [33].

5 Results and discussion

Section 5 is dedicated to reviewing the results of the visualisation tool, which first transforms the simulation data into Galactic coordinates and subsequently projects them onto an all-sky Mollweide projection map. For this purpose, in Section 5.1, the properties of the simulated stellar wakes are examined and the methodology is validated through comparison with previous work. Additionally, in Section 5.2, the stellar wakes generated by perturbers with different density profiles are analysed and visualised in Mollweide maps, and the broader implications of these findings are discussed.

5.1 Projection of the stellar wake and comparison against previous literature

One of the aims of this thesis was to create a tool to generate visualisations of stellar wake simulations. In order to visualise the simulation results, the following steps were required (see Section 4):

- Identification of the angle between the velocity of the perturber in the simulation box and the velocity of the perturber in the galaxy (the LMC),
- Performance of a series of coordinate transformations in the form of a rotation and translation to set the data into a Galactocentric frame of reference (coordinate origin at the center of the MW),
- Conversion from the Galactocentric frame of reference into a Galactic frame of reference (coordinate origin at the center of the Solar system),
- Generation of the Mollweide projection of the resulting data.

The output of the tool is shown and discussed in Section 5.1.1. Then, in order to check the validity of the tool, the resultant simulated wakes are compared with the results of Foote et al. [22], both before and after the Mollweide projection transformation process in Sections 5.1.2 and 5.1.3 respectively, to verify that the tool works as expected.

5.1.1 Mollweide projection of the simulated stellar wake

Figure 7 presents the resulting all-sky overdensity map of the stellar wake in Galactic coordinates after $0.7\ \mathrm{Gyr}$ of evolution. This is obtained by applying the transformation pipeline to the Hernquist density profile data. The wake is displayed trailing the LMC. An additional weaker overdensity is observed in and around the origin of the plot, believed to be a result of a projection effect. When projecting a homogeneous stellar background into the Mollweide projection using the same

transformation pipeline as described in Section 4, the resulting plot, Figure 12, bears a large resemblance to the additional overdensity observed near the origin in Figure 7 (The projection effect plot can be seen in Appendix 2 in Figure 12).

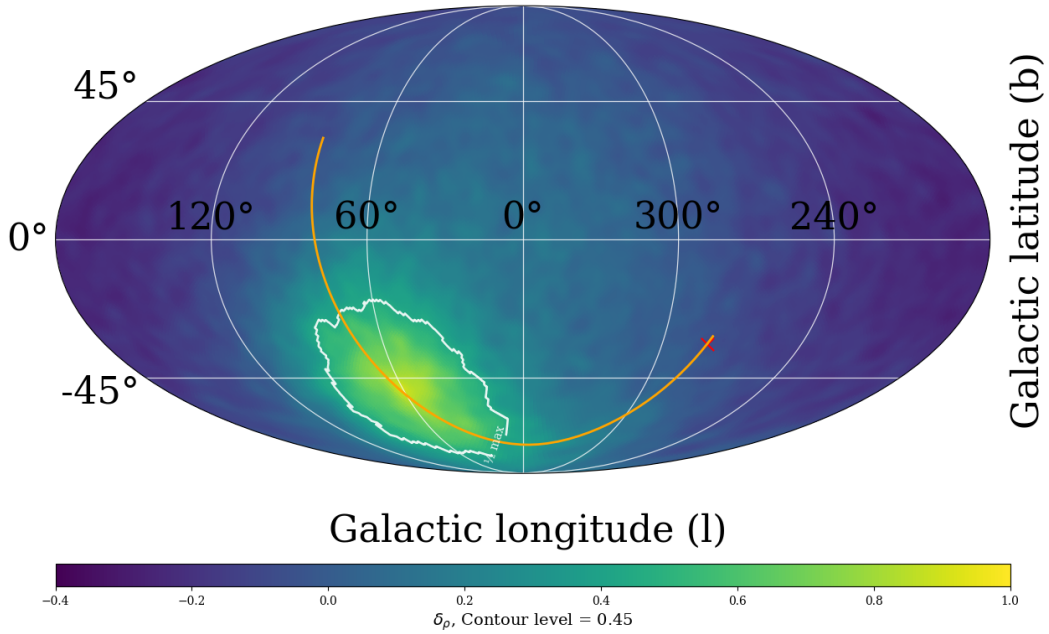

Figure 7. Mollweide projection of the simulated stellar wake induced by the LMC, assuming a Hernquist profile for its DM halo. The overdensity is highlighted by a white contour positioned at the calculated half-max value of 0.45. The trajectory of the LMC is marked with an orange line crossing the southern Galactic hemisphere and the current-day position of the LMC is marked by a red cross in the southeast section of the plot. The trajectory and position data was taken from the work of Vasiliev et al. [30]. The colorbar values were fixed between $-0.4 \ldots 1.0$ as seen in the result of Foote et al. [22] for a better comparison.

Figure 7 features data with a distance cut of $r \in [70, 100]$ kpc from the Galactic center for an isolated view of the wake. The bin size is $\sim 0.92°$ and the density map is smoothed by a Gaussian kernel with $\sigma = 2.12°$. The orange curved line shows the simulated trajectory of the LMC obtained from Vasiliev et al. [30], with a red cross marking the LMC's current-day position in the sky. The stellar wake is enclosed by a white contour with values higher than 0.45 inside of it, corresponding to the calculated half-maximum of the overdensity. The wake appears as an overdense region in the Galactic southwest, ranging from $l \in\sim [0, 100]$ and $b \in\sim [-30, -80]$. The wake appears slightly teardrop-shaped, featuring a distinctive higher overdensity near the center of the structure. The wake is wider near the Galactic plane and tapers off at the end nearer to the LMC.

5.1.2 Simulation box comparison

In this section, the simulation data used in this thesis is compared to the results seen in Foote et al. [22] to verify the simulation process. Observing and verifying the raw simulation data before any data transformations is important for two reasons: first, it gives an overview of what the data looks like before and after the transformations, as the Mollweide projection is not an intuitive projection type and is that much harder to understand without any previous reference. Secondly, verifying

the data with respect to previous literature helps to disentangle any differences in the final all-sky maps. Confirming whether the simulation results match up to a certain threshold signals that any deviations in the all-sky maps down the line will be due to differences in the transformation process rather than the input data.

Figure 8 shows the results of this work's stellar wake windtunnel simulation box in comparison to Foote et al. [22] in a 2D histogram, both displaying an overdensity plot. Figure 8a features a 600×600 kpc plot in the xy-plane with a bin size of 2 kpc, a z-cut of $z \in [-60, 60]$, smoothed with a Gaussian kernel of $\sigma = 1$ kpc in order to visually match Foote et al. [22] results in Figure 8b for an easier comparison.

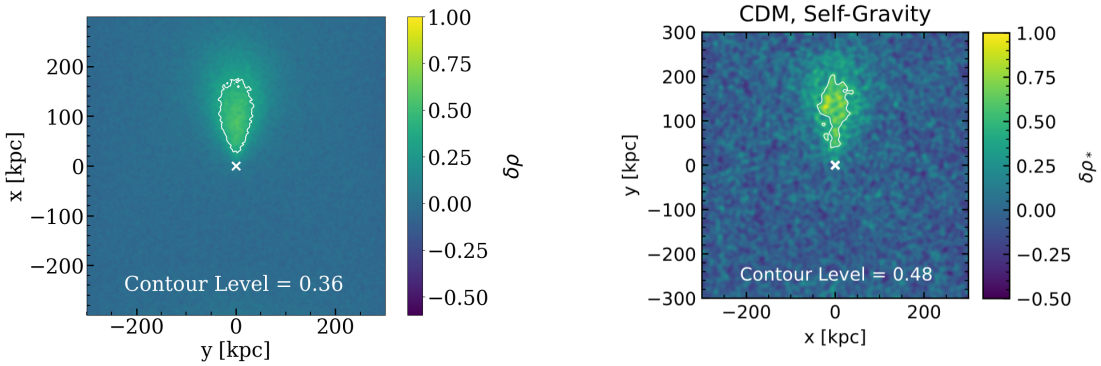

(a) A 2D histogram of this work's windtunnel simulation box in the xy plane

(b) A 2D histogram of Foote windtunnel simulation box in the xy plane

Figure 8. Comparison between the stellar wakes in the windtunnel simulation boxes of this work's results (left) and those of Foote et al. [22] (right). The half-max in Figure 8a is calculated to be at 0.36 and smoothed with a Gaussian kernel of $\sigma = 1$. The half-max in Figure 8b is calculated to be at 0.48 and the resulting density field is smoothed with a Gaussian kernel of $\sigma = 4$. The mismatch of the axes labels is purely a preferential matter, as Foote preferred to set the direction of LMC's resultant velocity vector as the y-axis while in this work's simulation it is set as the x-axis. This does not affect the results.

The granularity in Figure 8b can be explained by a lower stellar count used in their simulations. In their paper, Foote explains the process of creating their plot, mentioning that they used a ~ 100 times lower particle count than that of their DM simulations[1]. This may also explain the large difference between the half-max values, as a lower resolution field may produce sharper peaks in density. Additionally, this work's simulation's colorbar values have been set in a range of $-0.5 \ldots 1.0$, to match the colours observed in Foote simulations. In both figures, the wake is highlighted by a white contour and a white cross marks the location of the gravitational potential of the LMC. The contour levels are marked in the bottom section of the figures and denote the half-max values of the overdensities of the plots.

Despite the difference in overdensity, the wakes appear similar in size and shape, both reaching a length of ~ 200 kpc and a width of ~ 100 kpc. This suggests that the simulations, while produced with different N-body codes and with different simulated parameters (e.g., different

[1] Foote used $\sim 1.2 \times 10^6$ DM particles for their windtunnel simulatons. The estimated stellar particle count for Foote windtunnel simulations was $\sim 1.2 \times 10^4$ as opposed to this work simulation's stellar particle count of 1.342×10^8.

particle resolution), produce similar results.

5.1.3 Mollweide projection comparison

After validating the simulation outputs, the next step is to compare the final all-sky Mollweide maps of this work (Section 5.1.1) with those of Foote et al. [22]. This section reviews the all-sky Mollweide map obtained by Foote et al. [22] and presents the differences between the two works.

Figure 9 shows the Foote et al. [22] resultant stellar wake overdensity map projected into a Mollweide projection. As with Figure 7, the wake is highlighted by a white contour, where the calculated half-max is given as $\delta\rho_* > 0.34$. The white lines represent the trajectories of the LMC, the solid line being the windtunnel simulation trajectory and the dotted line representing results from a reference simulation[2]. The position of the LMC is not marked. The wake appears in the southwestern region of the sky from $l \in\sim [0, 120]$ and $b \in\sim [-80, 0]$.

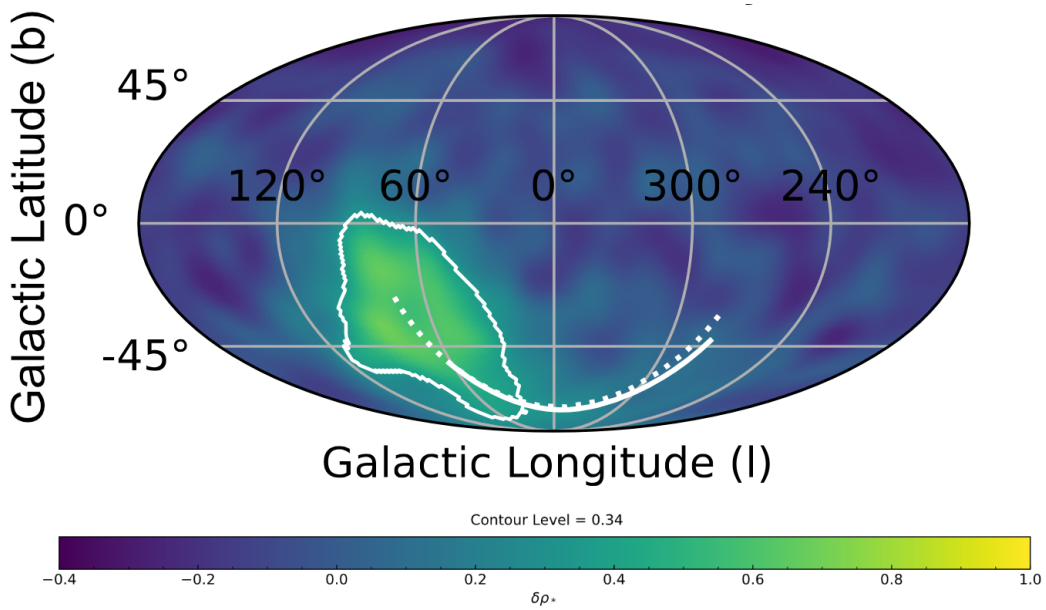

Figure 9. Mollweide projection by Foote et al. [22] of the simulated stellar wake induced by the LMC, assuming a Hernquist profile for its DM halo [22].

When comparing Figure 9 to this work's simulation's results, seen in Figure 7, the most noticeable difference is in the size and shape between the two stellar wakes. Figure 9 shows a clearly larger wake with a lower half-max value than that of this work's simulated wake. In Figure 7, the wake has a more teardrop shape and is much shorter in length in the Galactic latitude direction. A higher half-max value results in a smaller area covered by the contour[3]. Figure 9 seems to lack a higher central overdensity region, as is observed in this work's results, though this may be the result of a difference in resolution and smoothing levels, an additional projection effect, or the combination of those two options.

[2]Further reading about this available in Foote et al. [22]

[3]When adjusting the contour level to match the level seen in Foote et al. [22], the wake grows larger in size, as expected, and starts to resemble the wake seen in Fig 9

Despite the differences in the wake structures, the overall positions and morphology of the wake in both images are similar. This suggests that the visualisation tool works as intended, producing results similar to previously published works. While the main objective of the thesis has been completed, additional work may be required to eliminate the projection effect seen in Figures 7 and 12.

5.2 Comparison between cuspy and core subhalo density profiles

An additional contribution of this thesis is in the form of the comparison between the Hernquist and Plummer profiles, as this sort of comparison has not yet been made and can help assess whether the stellar wake of the LMC can be used to distinguish between cored and cuspy dark matter halos. As mentioned in Section 2.3, the difference in these profiles is expressed in the difference of the central region densities. The Hernquist profile (cusp) has a higher density peak in the middle followed by a sharp reduction in density, while the Plummer profile (core) displays a plateau followed by a shallower drop in density as the radius increases.

This distinction is particularly relevant in the context of the core-cusp discrepancy, where ΛCDM DM-only simulations predict cuspy inner density profiles, while observations of dwarf galaxies often favour cored distributions [2].

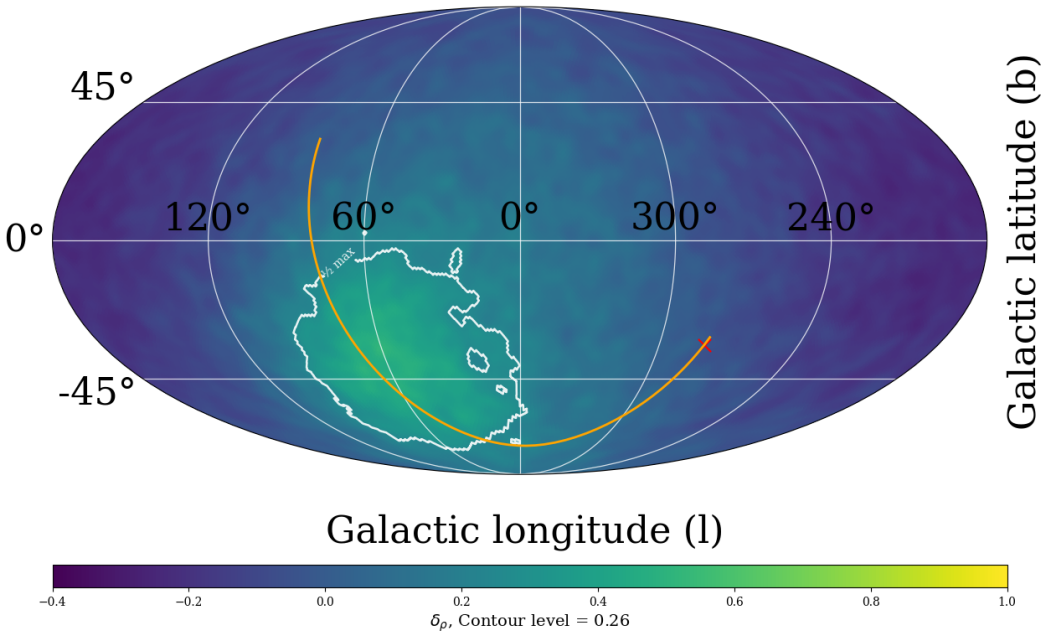

Figure 10. Mollweide projection of the simulated stellar wake induced by the LMC, assuming a Plummer profile for its DM halo. The overdensity is observed in the southwestern sector and is highlighted by a white contour positioned at the calculated half-max value of 0.26. The trajectory of the LMC is marked with an orange line crossing the southern Galactic hemisphere and the current-day position of the LMC is marked by a red cross in the southeast section of the plot.

The transformed stellar wake induced by the perturber with a Plummer density profile is seen in Figure 10. The figure features the same LMC trajectory data, similar to Figure 7. A large

overdensity is seen in the southwestern sector, ranging from $l \in\sim [0, 100]$ and $b \in\sim [-80, 0]$. The wake is highlighted by a contour at the calculated half-max value.

Compared to the Hernquist equivalent, the wake appears more granular in nature and even has pockets of low-density areas seen within the wake structure, as well as higher density islands separated from the main overdense region. The Plummer wake is more spread out than the Hernquist, covering a larger area in the sky, as well as lacks the distinctive high-density region seen in Figure 7, which, given the nature of the Plummer profile, is expected.

The lack of this high density region can be explained when examining Figure 11c, which shows the residual 2D overdensity maps induced by the different density profiles. The plot is presented in a simulation box reference frame, as it is a more intuitive way to present this difference, compared to a Mollweide map. Figure 11c shows a residual map, where the Plummer profile has been subtracted from the Hernquist profile. The figure highlights the differences in the densities of these profiles.

The residual map features a distinctive overdense island $\sim 150\ \mathrm{kpc}$ in length and $\sim 100\ \mathrm{kpc}$ in width near the middle of the wake region. Outside, surrounding the island, a large underdense area is visible, indicating that the Plummer profile produces a stronger density response outside the area, while the density inside the island is dominated by the Hernquist profile. This behaviour is to be expected when subtracting the Plummer induced wake from the Hernquist. Since the density of the Hernquist profile near its central region is much higher, an intuitive expectation would be to see a stronger gravitational pull near the region when compared to Plummer. This is precisely what the residual map highlights. The higher central density of the Hernquist induced wake produces the distinctive peak visible in Figure 7, which is correspondingly absent from the Plummer induced wake in Figure 10

The differences observed between the Hernquist and Plummer density profiles have direct implications in future observational searches. In the case of the LMC, the simulations of the stellar wakes show a clear distinction between the two density profiles when observed in the frame of reference of the Earth. When observed on the celestial sphere, the Hernquist wake appears smaller in the sky, but the stronger overdensity makes it easier to detect. A Plummer wake, on the other hand, covers a larger area, but due to a more spread-out structure, may cause difficulties in detection. This suggests that the morphology of the detected wake serves as an indirect probe into the density structure of the LMC's DM halo and may contribute to the core-cusp problem as well.

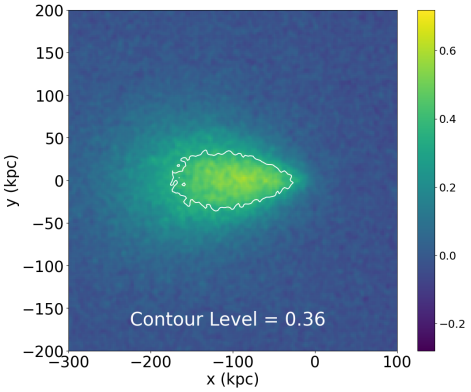

(a) Hernquist overdensity

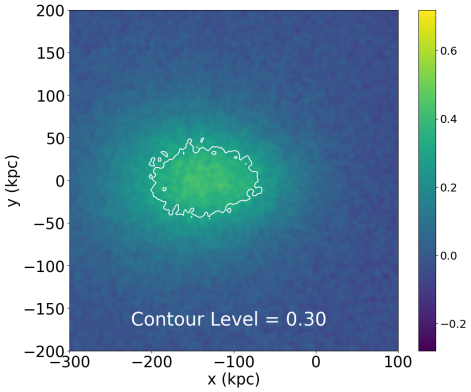

(b) Plummer Profile

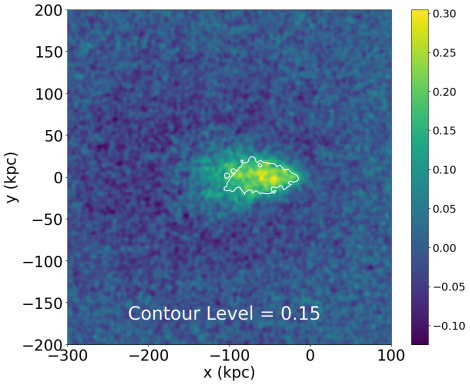

(c) Residual Overdensity map
(Hernquist-Plummer)

Figure 11. 11a and 11b show overdensity maps of the simulation outputs before the transformations. 11a features a simulated perturber induced stellar wake with a Hernquist profile, $\sim 100\ \mathrm{kpc}$ wide and $\sim 300\ \mathrm{kpc}$ long. The wake has a shape resembling a teardrop, with the pointier end facing the direction of movement. There's also a distinct overdense region near the middle of the wake. 11b shows a perturber induced stellar wake with a Plummer profile, $\sim 200\ \mathrm{kpc}$ wide and $\sim 300\ \mathrm{kpc}$ long. The wake is more round and spread out than the Hernquist wake. 11c shows a residual map when subtracting the Plummer profile from the Hernquist profile. The plots are focused on the overdense regions between $x \in [-300, 100]$ and $y \in [-200, 200]$.

6 Summary

The search for dark matter is an ongoing effort to constrain the microphysics of the dark matter particle. The difficulties in directly detecting the particle have led researchers to look into indirect methods to study the nature of the particle. One such method, a new and promising avenue for dark matter research, is the detection of stellar wakes.

The first aim of this thesis was to create a visualisation tool to project simulated windtunnel-style stellar wake data into a Galactic reference frame. The aim was achieved by implementing a transformation pipeline in Python, which included a set of translations and rotations, to transform the data into a Galactic frame of reference. An additional step was making a distance cut of the data to isolate the wake for better visibility. Then the data was projected onto an all-sky Mollweide projection map, displaying a 2D histogram of the overdensity of the simulated stellar wake.

To validate the transformation pipeline, the results were compared with previous literature. The general morphology as well as the location of the simulated stellar wake both before and after the transformation process shows a high level of similarity between the results of Foote et al. [22] and that of the simulated data used in this work. This shows that the transformation tool works as initially intended.

The second goal was to assess the possibility to discriminate between different density DM halo profiles. This was achieved by comparing the simulated wakes induced by the Hernquist (cusp) and Plummer (core) density profiles, which revealed two key differences between the wakes. The Plummer wake is larger and more diffuse than the Hernquist wake, and the Hernquist wake has a high overdensity near the middle. These results have shown that the different density DM halo profiles in an idealised setup are distinguishable from one another. Difficulties could arise when trying to observe the wakes in a real setting, as wakes are not easily identified from the background, either due to noise or poor signal quality. However, as a wake has tentatively been detected trailing the LMC in the work of Conroy et al. [27], the results presented by Conroy can in principle be used to constrain the inner structure of the LMC's DM halo. The results of this work are not contained to the context of the LMC, but are also relevant for DM halo and subhalo research in general.

While it is shown that the tool produces reliable results, it is noted that there is an additional overdensity observed near and around the origin of the plot. This is attributed to being a projection effect, which can be tackled in the future. The work in this thesis can be further expanded upon by comparing observational data from the work of Conroy et al. [27] with the results of this work to constrain the nature of the DM halo of the LMC.

Acknowledgements

I would like to thank my supervisors Sven Põder and Maria Jóse Benito Castaño for their guidance, and support throughout the writing of this Bachelor's thesis. I'm grateful for their constructive comments, friendly discussions, and encouragement which helped shape this work.

Acknowledgement of tools

The following tools have been used during the writing of this thesis:

- Anthropic's Claude (models Opus 4.6 and 4.7) was used for grammar and flow correction,
- Affinity Photo (version 1.10.6.1665) and Gimp (version 3.0.4) were used for editing images used in this thesis.

References

[1] Ignacio Ferreras. *Fundamentals of Dark Matter*. London: UCL Press, 2025.

[2] James S. Bullock and Michael Boylan-Kolchin. “Small-Scale Challenges to the CDM Paradigm”. In: *Annual Review of Astronomy and Astrophysics* 55.1 (Aug. 2017), pp. 343–387. ISSN: 1545-4282. DOI: 10.1146/annurev-astro-091916-055313. URL: http://dx.doi.org/10.1146/annurev-astro-091916-055313.

[3] Jo Bovy et al. “THE SHAPE OF THE INNER MILKY WAY HALO FROM OBSERVATIONS OF THE PAL 5 AND GD–1 STELLAR STREAMS”. In: *The Astrophysical Journal* 833.1 (Dec. 2016), p. 31. ISSN: 1538-4357. DOI: 10.3847/1538-4357/833/1/31. URL: http://dx.doi.org/10.3847/1538-4357/833/1/31.

[4] Malte Buschmann et al. “Stellar Wakes from Dark Matter Subhalos”. In: *Physical Review Letters* 120.21 (May 2018). ISSN: 1079-7114. DOI: 10.1103/physrevlett.120.211101. URL: http://dx.doi.org/10.1103/PhysRevLett.120.211101.

[5] Heinz Andernach and Fritz Zwicky. *English and Spanish Translation of Zwicky's (1933) The Redshift of Extragalactic Nebulae*. 2017. arXiv: 1711.01693 [astro-ph.IM]. URL: https://arxiv.org/abs/1711.01693.

[6] Barbara Ryden. *Introduction to Cosmology*. 2nd ed. Cambridge University Press, 2016.

[7] Edwin Hubble and Milton L Humason. “The velocity-distance relation among extra-galactic nebulae”. en. In: *Astrophys. J.* 74 (July 1931), p. 43.

[8] R. Clausius. “XVI. On a mechanical theorem applicable to heat”. In: *The London, Edinburgh, and Dublin Philosophical Magazine and Journal of Science* 40.265 (1870), pp. 122–127. DOI: 10.1080/14786447008640370. eprint: https://doi.org/10.1080/14786447008640370. URL: https://doi.org/10.1080/14786447008640370.

[9] Gianfranco Bertone and Dan Hooper. “History of dark matter”. In: *Reviews of Modern Physics* 90.4 (Oct. 2018). ISSN: 1539-0756. DOI: 10.1103/revmodphys.90.045002. URL: http://dx.doi.org/10.1103/RevModPhys.90.045002.

[10] Jacqueline Mitton. “How Vera Rubin encountered dark matter”. In: *Astronomy Geophysics* 62.2 (Apr. 2021), pp. 2.22–2.28. ISSN: 1366-8781. DOI: 10.1093/astrogeo/atab055. eprint: https://academic.oup.com/astrogeo/article-pdf/62/2/2.22/36614524/atab055.pdf. URL: https://doi.org/10.1093/astrogeo/atab055.

[11] Albert Bosma. *Rotation curves and the dark matter problem*. 2023. arXiv: 2309.06390 [physics.pop-ph]. URL: https://arxiv.org/abs/2309.06390.

[12] Jaan Einasto, Ants Kaasik, and Enn Saar. “Dynamic evidence on massive coronas of galaxies”. In: *Nature 1974 250:5464* 250 (5464 1974), pp. 309–310. ISSN: 1476-4687. DOI: 10.1038/250309a0. URL: https://www.nature.com/articles/250309a0.

[13] J P Ostriker, P J E Peebles, and A Yahil. “The size and mass of galaxies, and the mass of the universe”. In: *Astrophys. J.* 193 (Oct. 1974), p. L1.

[14] Jesús Zavala and Carlos S. Frenk. *Dark matter haloes and subhaloes*. 2019. arXiv: 1907.11775 [astro-ph.CO]. URL: https://arxiv.org/abs/1907.11775.

[15] George R Blumenthal et al. “Formation of galaxies and large-scale structure with cold dark matter”. en. In: *Nature* 311.5986 (Oct. 1984), pp. 517–525.

[16] Jaan Einasto. *Dark Matter*. 2010. arXiv: 0901.0632 [astro-ph.CO]. URL: https://arxiv.org/abs/0901.0632.

[17] Jorge Sánchez Almeida, Ignacio Trujillo, and Angel R. Plastino. "The Stellar Distribution in Ultrafaint Dwarf Galaxies Suggests Deviations from the Collisionless Cold Dark Matter Paradigm". In: *The Astrophysical Journal Letters* 973.1 (Sept. 2024), p. L15. DOI: 10.3847/2041-8213/ad66bc. URL: https://doi.org/10.3847/2041-8213/ad66bc.

[18] Se-Heon Oh et al. "HIGH-RESOLUTION MASS MODELS OF DWARF GALAXIES FROM LITTLE THINGS". In: *The Astronomical Journal* 149.6 (May 2015), p. 180. DOI: 10.1088/0004-6256/149/6/180. URL: https://doi.org/10.1088/0004-6256/149/6/180.

[19] BI Xiaojun. *Detection of Dark Matter Particles and Progress - Bulletin of the Chinese Academy of Sciences*. URL: http://www.bcas.cas.cn/perspective/201905/t20190517_209846.html.

[20] J. Bovy. *Dynamics and Astrophysics of Galaxies*. Princeton, NJ: Princeton University Press, in press 2026.

[21] Lars Hernquist. "An analytical model for spherical galaxies and bulges". In: *Astrophys. J.* 356 (June 1990), p. 359.

[22] Hayden R. Foote et al. "Structure, Kinematics, and Observability of the Large Magellanic Cloud's Dynamical Friction Wake in Cold versus Fuzzy Dark Matter". In: *The Astrophysical Journal* 954.2 (Sept. 2023), p. 163. ISSN: 1538-4357. DOI: 10.3847/1538-4357/ace533. URL: http://dx.doi.org/10.3847/1538-4357/ace533.

[23] H. C. Plummer. "On the Problem of Distribution in Globular Star Clusters: (Plate 8.)" In: *Monthly Notices of the Royal Astronomical Society* 71.5 (Mar. 1911), pp. 460–470. ISSN: 0035-8711. DOI: 10.1093/mnras/71.5.460. eprint: https://academic.oup.com/mnras/article-pdf/71/5/460/2937497/mnras71-0460.pdf. URL: https://doi.org/10.1093/mnras/71.5.460.

[24] Põder, Sven et al. "Detection of stellar wakes in the Milky Way: A deep learning approach". In: *AA* 693 (2025), A227. DOI: 10.1051/0004-6361/202451480. URL: https://doi.org/10.1051/0004-6361/202451480.

[25] S Chandrasekhar. "Dynamical friction. I. general considerations: The coefficient of dynamical friction". en. In: *Astrophys. J.* 97 (Mar. 1943), p. 255.

[26] Nicolas Garavito-Camargo et al. "Hunting for the Dark Matter Wake Induced by the Large Magellanic Cloud". In: *The Astrophysical Journal* 884.1 (Oct. 2019), p. 51. ISSN: 1538-4357. DOI: 10.3847/1538-4357/ab32eb. URL: http://dx.doi.org/10.3847/1538-4357/ab32eb.

[27] Charlie Conroy et al. "All-sky dynamical response of the Galactic halo to the Large Magellanic Cloud". In: *Nature* 592.7855 (Apr. 2021), pp. 534–536. ISSN: 1476-4687. DOI: 10.1038/s41586-021-03385-7. URL: http://dx.doi.org/10.1038/s41586-021-03385-7.

[28] Nitya Kallivayalil et al. "THIRD-EPOCH MAGELLANIC CLOUD PROPER MOTIONS. I. HUBBLE SPACE TELESCOPE/WFC3 DATA AND ORBIT IMPLICATIONS". In: *The Astrophysical Journal* 764.2 (Feb. 2013), p. 161. DOI: 10.1088/0004-637X/764/2/161. URL: https://doi.org/10.1088/0004-637X/764/2/161.

[29] Douglas Potter, Joachim Stadel, and Romain Teyssier. *PKDGRAV3: Beyond Trillion Particle Cosmological Simulations for the Next Era of Galaxy Surveys*. 2016. arXiv: 1609.08621 [astro-ph.IM]. URL: https://arxiv.org/abs/1609.08621.

[30] Eugene Vasiliev and Holger Baumgardt. “Gaia EDR3 view on galactic globular clusters”. In: *Monthly Notices of the Royal Astronomical Society* 505.4 (May 2021), pp. 5978–6002. ISSN: 1365-2966. DOI: 10.1093/mnras/stab1475. URL: http://dx.doi.org/10.1093/mnras/stab1475.

[31] James E. Gentle. *Matrix Algebra: Theory, Computations, and Applications in Statistics*. URL: https://books.google.ee/books?id=PDjIV0iWa2cC&pg=PA172&redir_esc=y#v=onepage&q&f=false.

[32] Joseph Rabinoff Dan Margalit. *Orthogonal Projection*. URL: https://textbooks.math.gatech.edu/ila/projections.html.

[33] John P Snyder. “Map Projections-A Working Manual”. In: *U.S. Geological Survey Professional Paper 1395* (1987).

Abstract

The ΛCDM cosmological model successfully predicts the evolution and the large-scale structure of the Universe, but struggles to define the process on Galactic and subgalactic scales. Galaxies are believed to be surrounded by dark matter halos, in which the properties of dark matter are encoded. Analysing stellar wake morphology offers a promising way to probe the structure of dark matter halos surrounding galaxies. This thesis develops a Python-based visualisation tool to transform windtunnel-style N-body simulation data of the Large Magellanic Cloud (LMC) into all-sky Mollweide projections in Galactic coordinates. Simulations used in this thesis were provided for the Hernquist and Plummer density profiles. The data was processed through a series of coordinate transformations and projected into a Galactic frame of reference. The tool successfully reproduces the stellar wake morphology and sky position reported in previous literature. Further analysis between the stellar wake simulations produced with different density profiles shows that the stellar wake of the LMC can be used to discriminate between cored and cuspy dark matter halo profiles. This demonstrates that the stellar wake morphology offers a viable observational probe in the ongoing investigations of dark matter properties at Galactic scales.

The thesis is in English and contains 21 pages of text, 6 chapters, 12 figures, 1 table.

Annotatsioon

ΛCDM kosmoloogiline mudel ennustab edukalt Universumi evolutsiooni ja suuremastaabilist struktuuri, kuid galaktikate skaalal on endiselt palju lahendamata probleeme. Praeguse arusaama kohaselt on galakikad ümbritsetud tumeaine halodega, millesse on kodeeritud tumeaine omadusi. Tähiskiilude morfoloogia analüüsimine on paljulubav meetod tumeaine halode kohta rohkem teada saada. Käesoleva lõputöö raames arendatakse välja programmeerimiskeele *Python* baasil visualiseerimise tööriist, mis transformeerib Suure Magalhãesi Pilve (LMC) tuuletunneli stiilis N-keha simulatsiooni andmed galaktilistesse koordinaatidesse *Mollweide*'i projektsioonis. Simulatsioonid tehti PKDGRAV3 abil, millega loodi Hernquisti ja Plummeri tihedusprofiilide poolt indutseeritud andmestikud. Andmed töödeldi koordinaattransformatsioonide kaudu ja projetseeriti galaktilisse taustsüsteemi. Võttes võrdluseks varasemas kirjanduses esinenud tulemused, suudab tööriist edukalt replitseerida tähiskiilu morfoloogia ja positsiooni taevas. Erinevate tihedusprofiiliga simulatisoonide vaheline analüüs näitab, et LMC tähiskiilu saab efektiivselt kasutada erinevate tihedusprofiilide poolt indutseeritud tähiskiilude eristamiseks. See viitab, et tähiskiilu morfoloogia uurimine on pädev meetod vaatluslikult piirata tumeaine olemust galaktilisel skaalal.

Lõputöö on kirjutatud inglise keeles ning sisaldab teksti 21 leheküljel, 6 peatükki, 12 joonist, 1 tabel.

Appendices

Appendix 1 – Non-exclusive licence for reproduction and publication of a graduation thesis[1]

I Daniel Nurme

1. Grant Tallinn University of Technology free licence (non-exclusive licence) for my thesis "Visualising the Milky Way response to the infall of the Large Magellanic Cloud", supervised by Sven Põder and María José Benito Castaño
    1.1. to be reproduced for the purposes of preservation and electronic publication of the graduation thesis, incl. to be entered in the digital collection of the library of Tallinn University of Technology until expiry of the term of copyright;
    1.2. to be published via the web of Tallinn University of Technology, incl. to be entered in the digital collection of the library of Tallinn University of Technology until expiry of the term of copyright
2. I am aware that the author also retains the rights specified in clause 1 of the nonexclusive licence.
3. I confirm that granting the non-exclusive licence does not infringe other persons' intellectual property rights, the rights arising from the Personal Data Protection Act or rights arising from other legislation.

25.05.2026

[1] The non-exclusive licence is not valid during the validity of access restriction indicated in the student's application for restriction on access to the graduation thesis that has been signed by the school's dean, except in case of the university's right to reproduce the thesis for preservation purposes only. If a graduation thesis is based on the joint creative activity of two or more persons and the co-author(s) has/have not granted, by the set deadline, the student defending his/her graduation thesis consent to reproduce and publish the graduation thesis in compliance with clauses 1.1 and 1.2 of the non-exclusive licence, the non-exclusive licence shall not be valid for the period.

Appendix 2 – Additional Plots

Transformation of the Homogeneous Stellar Background Data

In this Appendix, the homogeneous stellar background data used in the windtunnel simulation is transformed using the same transformation pipeline described in Section 4.

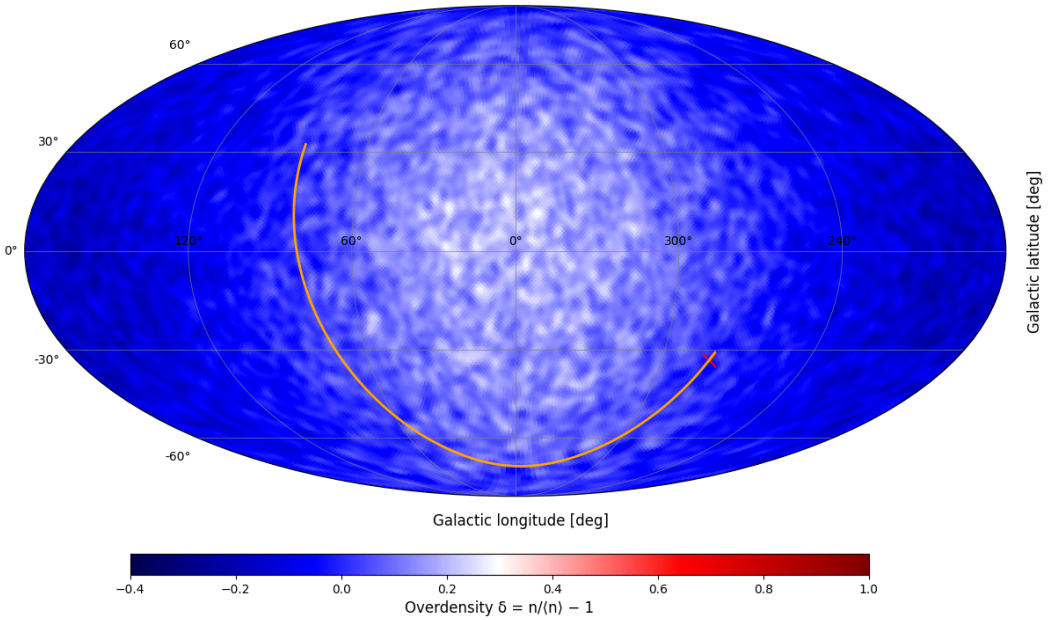

Figure 12. Mollweide projection of the homogeneous stellar background data showing the projection effect described in Section 5.1.1.

Figure 12 shows a Mollweide projection of the homogeneous stellar background data. An overdense region is observed in the origin of the plot, likely due to a projection effect occurring as a result of plotting a 3D sphere on a 2D surface. This projection effect seems to be the cause for the additional overdensity in Figure 7.